

A New Algorithm for the Thermo-Mechanical Coupled Frictional Contact Problem of Polycrystalline Aggregates Based on Plastic Slip Theory

Yun Chen¹, Junzhi Cui², Yufeng Nie¹ and Yiqiang Li¹

Abstract: This paper presents a new numerical algorithm for thermal-mechanical coupled analysis of polycrystalline aggregates based on the plastic slip theory inside crystals and the frictional contact on their interfaces. It involves the mechanics and heat conduction behaviors caused by both force loads and temperature changing within crystal and contact interfaces between crystals. Firstly, the constitutive relationship inside single crystal, and the moment equations and energy equations are derived by means of rate-dependent plastic deformation theory and the formulation of elastic-plastic tangent modulus depended on temperature. Secondly, the contact conditions with friction, including frictional heat generation and heat transfer across the contact interface, are discussed. And then based on the ABAQUS software, the subroutines to calculate thermo-mechanical behaviors of polycrystalline copper are coded, and a polycrystalline body composed by four grains within 16 contact interfaces is simulated under the torsion and bending loadings. The numerical results show that crack propagation path are associated with loading ways and temperature change through the contact interfaces in addition to the friction heat generation. The displacement jumps are related to the contact pressure. The modeling approach presented in this work can be extended to more complicated systems with the interaction of a number of grains.

Keywords: Polycrystalline aggregates, Friction contact, Thermo-mechanical coupled, Crystal slip theory.

1 Introduction

Thermo-mechanical coupled problems are often encountered in civil, mechanical or aerospace engineering. The coupling between the mechanics and thermal behav-

¹ Department of Applied Mathematics, School of Science, Northwestern Polytechnical University, Xi'an 710129, China. E-mail: ychensate@163.com

² LSEC, ICMSEC, Academy of Mathematics and System Sciences, Chinese Academy of Sciences, Beijing, 100190, China.

iors is twofold. On the one hand, the deformation of the structure strongly depends on the temperature field. On the other hand, deformations induce structural heat behaviors. So it is necessary to discuss the behaviors of polycrystalline body in the thermo-mechanical coupled environment. The evolution of the deformation field and the temperature field is typically accompanied with the local rearrangement of in-homogeneities in the crystal interiors. The formulas of elastic-plastic tangent modulus depended on temperature are derived in our previous work [Chen, Cui, Nie, and Guan (2011)], some main results are briefly shown here to simulate the thermal-mechanical coupled frictional contact behaviors of polycrystalline. Relative to the microcrystalline counterparts from the atomistic simulations reported in recent literatures [Tian and Cui (2010)], the results show that local stress concentrations are driven by dislocation mechanisms. It is clear that slip and separation phenomena begin to play an important role on the interfaces of crystals for the polycrystalline materials. To the knowledge of the authors there are two methods to simulate the crystal boundary phenomena at continuum sense. One method assumes that the interfaces between the crystals are sandwich materials with certain thickness, and the boundary regions were modeled by adding an expanded strain perpendicular to crystal interface to internal slip deformation, this approach can be seen in our work [Chen, Cui, Nie, and Guan (2011)]. Another approach to treat interfaces is to construct the frictional contact algorithm on interfaces. In this paper the interface frictional contact algorithm is discussed.

The numerical simulation for frictional contact problems of polycrystalline aggregates is still a challenging task. Earlier works have been done to deal with the contact problems in friction and large deformations, those can be found in [Wriggers and Miehe (1994);Johansson and Klarbring (1993);Laursen (2003);Song and Yovanovich (1987)]. The large deformation based on the node to-segment algorithm of the contact interface between two bodies was adopted by Wriggers [Wriggers and Miehe (1994)], Lagrange multiplier technique was enforced on contact constraints [Nour-Omid and Wriggers (1986)],penalty methods is given in [Wriggers and Simo (1985)] and the contact smooth techniques for saving computational time is in the works of Belyschko and Neal[Belytschko and Neal (1991)]. In recent years the simulation of contact problems is still of intensive interest. Polycrystalline systems involving contact mechanics between grains were solved by Wei[Wei and Anand (2004)], the mortar approach for dynamic contact problems were found in [Hueber and Wohlmuth (2009)], and the hot metal forming [Adam and Ponthot (2002)], the contact friction model of large plastic deformation in powder compaction process [Khoei, Biabanaki, Vafa, Yadegaran, and Keshavarz (2009)]. Further, the contact algorithm was developed by Temizer[Temizer and Wriggers (2008)], they treated a contact homogenization technique with deformable elastic

solid and rigid surface. In addition, the extended finite element technique was applied to modeling contact problems by Khoei [Khoei, Biabanaki, and Anahid (2009)]. The challenges in solving the problems mentioned above are following: the contact constraints are strongly nonlinear and not smooth, the searching for contact need to be done efficiently, and the cost for numerical simulations is expensive. These issues are treated very carefully in this paper, the finite element meshes are finer on the contact surface than other regions, and the parallel computing is adopted on the cluster service to decrease computing time.

In this paper we mainly focus on a new computational algorithm for simulating the thermo-mechanical coupled problem with friction contact condition on the interface and thermo-elastic-plastic deformation in the crystal interiors at finite strains. The thermo-mechanical coupled governing equations of crystal, based on rate-dependent slip deformation theory, and thermodynamics law are given in section 2. In section 3 the coupled thermo-mechanical friction contact algorithm is described without physical softening, which is associated with large deformation and relative sliding. The numerical results for the thermo-mechanical coupled behavior of the polycrystalline at bending and torsion are shown in section 4. Finally, some concluding remarks are given.

2 Thermal-elasto-plasticity constitutive equations of single crystal

For the convenience of descriptions below, here the basic symbols are defined:

u	displacement	t	time
ρ_0	mass density	S	the second Piola-Kirchhoff stress
f	body force density	p	the first Piola-Kirchhoff stress
k	thermal conductivity coefficient	r	heat source density
γ	shear strain	c	specific heat
θ	absolute temperature	σ	cauchy-stress
∇	gradient operator	Div	divergence operator

2.1 Foundation of crystal plasticity

The multiplicative decomposition of deformation gradient F is expressed as

$$F = F^e F^p.$$

Where, F^e denotes lattice distortion and the rigid rotation that produced by the elastic deformation gradient, F^p denotes plastic shear of the material to an intermediate reference configuration in which lattice orientation and spacing are the same as in the original reference configuration. Each slip system is specified by a unit normal $n^{(\alpha)}$ to the slip plane, and a unit vector $s^{(\alpha)}$ denoting the slip direction.

Let L denotes velocity gradient, $L = \dot{F}F^{-1} = D + W$, the symmetric and skew parts of the velocity gradient are respectively denoted by deformation rate tensor D and spin rate tensor W , and their plastic parts are respectively written as D^p and W^p , have $D^p = \sum_{\alpha \in \mathcal{A}} P^{(\alpha)} \dot{\gamma}^{(\alpha)}$, $W^p = \sum_{\alpha \in \mathcal{A}} W^{(\alpha)} \dot{\gamma}^{(\alpha)}$, and corresponding elastic parts are denoted by D^e, W^e respectively. Where, $P^{(\alpha)} = \frac{1}{2}[s^{(\alpha)}n^{(\alpha)} + n^{(\alpha)}s^{(\alpha)}]$, $W^{(\alpha)} = \frac{1}{2}[s^{(\alpha)}n^{(\alpha)} - n^{(\alpha)}s^{(\alpha)}]$, and we denote the set of active systems by $\mathcal{A} = \{\alpha | \alpha = 1, \dots, m \leq n\}$.

2.2 Thermo-mechanical coupled equations

Refer to [Clayton (2005);Anand and Gurtin (2003)], the free energy in the current configuration is given by,

$$\psi = \frac{1}{2}E^e \cdot \mathcal{C}_e^\tau E^e - \mathcal{C}_e^\tau E^e a_0(\theta - \theta_0) + \frac{1}{2}\lambda\mu(\theta, \zeta)\zeta^2 + c(\theta - \theta_0) - c\theta \ln\left(\frac{\theta}{\theta_0}\right),$$

where, \mathcal{C}_e^τ is the elastic-plastic tangent modulus, E^e denotes elasticity Cauchy strain. a_0 is the thermal expansion tensor, θ_0 is the initial temperature, λ is a constant, $\mu(\theta, \zeta)$ is the equivalent shear modulus, ζ is an internal variable expression related crystal defect microscopic elastic storage energy. The term $\frac{1}{2}E^e \cdot \mathcal{C}_e^\tau E^e - \mathcal{C}_e^\tau E^e a_0(\theta - \theta_0)$ is the strain energy, this term $\frac{1}{2}\lambda\mu(\theta, \zeta)\zeta^2$ is the plastic energy and the term $c(\theta - \theta_0) - c\theta \ln\left(\frac{\theta}{\theta_0}\right)$ is the thermal energy.

And the second Piola-Kirchoff stress is given by $S = \mathcal{C}_e^\tau [E^e - a_0(\theta - \theta_0)]$, the term $\mathcal{C}_e^\tau a_0(\theta - \theta_0)$ reflects temperature induced thermal effects.

The momentum conservation equation in reference configuration is given by

$$Div p + f = \rho_0 \frac{\partial^2 u}{\partial t^2}. \tag{1}$$

Here, there is a certain relation between the first Piola-Kirchoff stress and the second Piola-Kirchoff stress, $p = FS$. The equation of heat in reference configuration is derived from the first thermodynamics, to express that equation as, see [Rosakis, Rosakis, Ravichandran, and Hodowany (2000);Adam and Ponthot (2005)] for more details.

$$c\dot{\theta} = \kappa(SD^p) + Div(k\nabla \cdot \theta) + r. \tag{2}$$

As the heat produced by elastic deformation is much smaller than that by the plastic deformation, so part from elastic deformation. The term $\kappa(SD^p)$ only describes non-elastic deformation energy, and the term $k\nabla \cdot \theta$ represents heat flux, κ the plastic power into heat ratio, located among 0.8 and 1.0 [Belytschko, Liu, and Moran

(2000)]. So the thermal-mechanical coupled equations can be written as

$$\begin{cases} \text{Div} F \{ \mathcal{C}_e^\tau [E^e - a_0(\theta - \theta_0)] \} + f = \rho_0 \frac{\partial^2 u}{\partial t^2}, \\ c\dot{\theta} = \kappa \left\{ [\mathcal{C}_e^\tau E^e - \mathcal{C}_e^\tau a_0(\theta - \theta_0)] \sum_{\alpha \in \mathcal{A}} P^{(\alpha)} \dot{\gamma}^{(\alpha)} \right\} + \text{Div}(k\nabla \cdot \theta) + r. \end{cases} \quad (3)$$

As the elastic-plastic tangent modulus needs to be updated at each increment step, here, next we give the derived process of elastic-plastic tangent modulus formula.

2.3 Constitutive relation

Generally think that the elastic properties of the crystal is not affected by the slip deformation, taking into account the impact of thermal stress, the elastic constitutive relation in the intermediate configuration is written as:

$$\mathcal{L}_v^e \sigma = \mathcal{C}_e^\tau : (D^e - a_0 \dot{\theta}). \quad (4)$$

Where, $\mathcal{L}_v^e \sigma$ is Jaumann rate of the Cauchy stress tensor which is the co-rotational stress rate in terms of the coordinate system that rotates with the lattice. $\mathcal{L}_v^e \sigma$ is determined by

$$\mathcal{L}_v^e \sigma = \dot{\sigma} - W^e \sigma + \sigma W^e. \quad (5)$$

The co-rotational stress rate on the coordinate system that rotates with the material is given as

$$\mathcal{L}_v \sigma = \dot{\sigma} - W \sigma + \sigma W. \quad (6)$$

Combining Eq. 4 and Eq. 6, rewrite the Eq. 5

$$\mathcal{L}_v^e \sigma = \mathcal{L}_v \sigma + \sum_{\alpha \in \mathcal{A}} B^{(\alpha)} \dot{\gamma}^{(\alpha)}. \quad (7)$$

In the Eq. 7, let

$$B^{(\alpha)} = W^{(\alpha)} \sigma - \sigma W^{(\alpha)}. \quad (8)$$

According to the Eq. 4-Eq. 8, so get

$$\mathcal{L}_v \sigma = \mathcal{C}_e^\tau : D^e - (\mathcal{C}_e^\tau : a_0 \dot{\theta}) - \sum_{\alpha \in \mathcal{A}} B^{(\alpha)} \dot{\gamma}^{(\alpha)}. \quad (9)$$

The Eq. 9 is coupled temperature, shear rate and stress rate, we compute the shear rate as expected now and then we update the elastic-plastic tangent modulus. The constitutive formulation in the present report adopts the rate-dependent hardening

model. The shear rate $\dot{\gamma}^{(\alpha)}$ of the α slip system in a rate-dependent crystalline solid is determined by the corresponding resolved shear stress $\tau^{(\alpha)}$, it is usually presented by a power function,

$$\dot{\gamma}^{(\alpha)} = \dot{a}^{(\alpha)} \left[\frac{\tau^{(\alpha)}}{g^{(\alpha)}} \right] \left[\left| \frac{\tau^{(\alpha)}}{g^{(\alpha)}} \right| \right]^{\frac{1}{m}-1}, \tag{10}$$

where the constant $\dot{a}^{(\alpha)}$ is the reference strain rate on slip system α , $g^{(\alpha)}$ is a variable which describes the current strength of that system, m is the rate sensitivity exponent. In the limit as $m \rightarrow 0$, this power law approaches that of a rate-independent material. The strain hardening is characterized by the evolution of the strengths $g^{(\alpha)}$ through the incremental relation:

$$\dot{g}^{(\alpha)} = \sum_{\beta \in \mathcal{A}} h_{\alpha\beta} \left| \dot{\gamma}^{(\beta)} \right|, \tag{11}$$

where, $h_{\alpha\beta}$ are the slip hardening moduli. We employ a linear interpolation within Δt , the increment shear strain $\Delta\gamma^{(\alpha)}$ in slip system α within the time increment Δt ,

$$\Delta\gamma^{(\alpha)} = \Delta t \left[(1 - \Theta) \dot{\gamma}_t^{(\alpha)} + \Theta \dot{\gamma}_{t+\Delta t}^{(\alpha)} \right]. \tag{12}$$

The parameter Θ belongs to $(0,1)$, it is chosen as 0.5 . The increment of shear strain $\Delta\gamma^{(\alpha)}$ in the slip systems are uniquely determined by the following linear algebraic equation,

$$\begin{aligned} & \sum_{\beta \in \mathcal{A}} \left(\delta_{\alpha\beta} + \frac{\Theta \Delta t \dot{\gamma}_t^{(\alpha)}}{m \tau^{(\alpha)}} [P^{(\alpha)} : \mathcal{C}_e^\tau + B^{(\alpha)}] : P^{(\beta)} + \frac{\Theta \Delta t \dot{\gamma}_t^{(\alpha)}}{m g^{(\alpha)}} h_{\alpha\beta} \text{sgn}(\tau^{(\beta)}) \right) \Delta\gamma^{(\beta)} \\ & = \left(\dot{\gamma}_t^{(\alpha)} + \frac{\Theta \Delta t \dot{\gamma}_t^{(\alpha)}}{m \tau^{(\alpha)}} \left\{ [P^{(\alpha)} : \mathcal{C}_e^\tau + B^{(\alpha)}] : D - P^{(\alpha)} : (\mathcal{C}_e^\tau : a_0 \dot{\theta}) \right\} \right) \Delta t \end{aligned} \tag{13}$$

Let $N_{\alpha\beta}$ be

$$\begin{aligned} N_{\alpha\beta} &= \delta_{\alpha\beta} + \frac{\Theta \Delta t \dot{\gamma}_t^{(\alpha)}}{m \tau^{(\alpha)}} \sum_{\beta \in \mathcal{A}} [P^{(\alpha)} : \mathcal{C}_e^\tau + B^{(\alpha)}] : P^{(\beta)} \\ &+ \frac{\Theta \Delta t \dot{\gamma}_t^{(\alpha)}}{m g^{(\alpha)}} \sum_{\beta \in \mathcal{A}} h_{\alpha\beta} \text{sgn}(\tau^{(\beta)}). \end{aligned} \tag{14}$$

Let $\Delta\gamma^{(\alpha)}$ substitute into Eq. 9 and by comparing the left and right sides of the equation, the expression of update elastic-plastic tangent modulus $\mathcal{C}_e^{\tau p}$ are given by

$$\mathcal{C}_e^{\tau p} = \mathcal{C}_e^{\tau} - \sum_{\alpha \in \mathcal{A}} \sum_{\beta \in \mathcal{A}} (\mathcal{C}_e^{\tau} : P^{(\alpha)} + B^{(\alpha)}) [N_{\alpha\beta}]^{-1} \frac{\Theta \Delta t \dot{\gamma}_t^{(\beta)}}{m\tau^{(\alpha)}} [P^{(\beta)} : \mathcal{C}_e^{\tau} + B^{(\beta)}]. \quad (15)$$

3 Thermo-mechanical coupled friction contact formulation on the interface

We limit the discussion to a two body system without loss of generality for defining the thermo-mechanical friction contact problems. The reference configurations of two bodies are denoted by the open sets Ω^m and Ω^s as shown in Fig. 1 and $\Omega^m \subset R^d, \Omega^s \subset R^d$. Where d is the number of spatial dimensions. The superscript m stands for the master body s for the slave body.

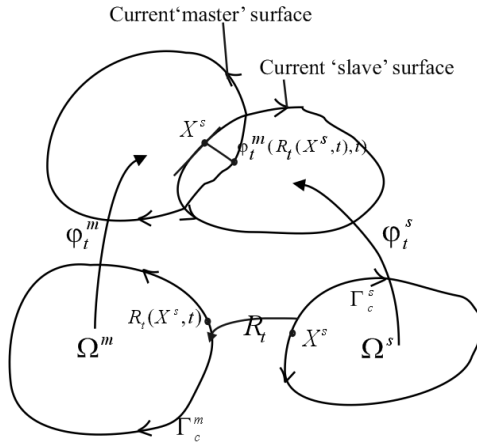


Figure 1: Basic contact geometry.

The bodies undergo motions are denoted by $\varphi_t^i, i \in (s, m)$, which cause them to contact during some portion of the time interval $[0, T]$. These motions can be expressed via the following mappings:

$$\varphi_t^{(i)} : x^i = \varphi^i(X^i, t), \quad i \in (s, m), t \in [0, T]. \quad (16)$$

Where, X is a point of reference configuration, at any time $t \in [0, T]$. Assume two bodies come into contact and view mechanical contact as a penetration of the current boundaries $\varphi_t^{(i)}(\Gamma_c^i)$, here, $\Gamma_c^i \subset \partial\Omega^i$ are possible contact surfaces of the bodies Ω^i . Denote the current slave surface $\varphi_t^{(s)}(\Gamma_c^s)$ penetrates into the current master surface $\varphi_t^{(m)}(\Gamma_c^m)$ and we take the latter as target. Define a smooth mapping

$R_t(X^s) : \Gamma_c^s \rightarrow \Gamma_c^m$, $X^s \in \Gamma_c^s$. The reference point X^s on the boundary Γ_c^s after deformation is projected onto the current master boundary $\varphi_t^{(m)}(R_t(X^s, t), t)$ along the current normal n^s . The relative displacement after local deformation from the point X^s on the contact surface of slave surface to the point on the contact surface of target may be defined as

$$g_n := [\varphi_t^s(X^s, t) - \varphi_t^{(m)}(R_t(X^s, t), t)] \cdot n \quad \text{on} \quad \Gamma_c = \Gamma_c^m \cap \Gamma_c^s, \quad (17)$$

here, g_n is the projection of the gap of two bodies on the normal direction, and $n := n^s$ is the normal vector of the current configuration. The contact conditions has the following expressions

$$g_n \leq 0, \quad p_n \geq 0, \quad p_n g_n = 0, \quad (18)$$

where p_n is the normal contact stress and may be defined as the form $p_n = \epsilon_n g_n$, ϵ_n is the normal stiffness of the material. The total contact stress p_c is defined as

$$p_c := -p_c^s n^s = p_c^m n^m \quad \text{on} \quad \Gamma_c^s, \quad (19)$$

and its tangential part

$$p_\tau := p_c - p_n. \quad (20)$$

We split the tangential part of the gap g_τ into elastic g_τ^e and plastic part g_τ^p . Define the temperature of interface $\theta_c := \max\{\theta_c^m, \theta_c^s\}$ and initial temperature is θ_0 . Next we introduce the free energy of the interface and it has the following form [Laursen (1999)],

$$\hat{\Psi}_c(g_n, g_\tau^e, \theta_c) = \left\{ \begin{array}{l} I_{R^-}(g_n) \text{ or} \\ \frac{1}{2} \epsilon_n \langle g_n \rangle^2 \end{array} \right\} + \frac{\epsilon_\tau}{2} \langle g_\tau^e \rangle^2 - \frac{c_c}{2\theta_0} (\theta_c - \theta_0)^2, \quad (21)$$

$$\text{with } I_{R^-}(g_n) = \begin{cases} 0 & g_n \leq 0 \\ +\infty & g_n > 0 \end{cases}, \quad \langle \cdot \rangle = \max(0, \cdot),$$

where, c_c is heat capacity of the contact interface and ϵ_τ is think as physical tangential stiffness, $I_{R^-}(g_n)$ indicates that infinite stiffness of the interface in the normal direction. The conditions for the heat flux $q_c^i := q^i n^i$ across the possible contact interface and may be written as:

$$\begin{aligned} q_c^m &= \frac{k^m(p_n)k^s(p_n)}{k^m(p_n) + k^s(p_n)} (\theta_c^m - \theta_c^s) - \frac{k^m(p_n)}{k^m(p_n) + k^s(p_n)} \mathcal{D}_{mech,c}, \\ q_c^s &= \frac{k^m(p_n)k^s(p_n)}{k^m(p_n) + k^s(p_n)} (\theta_c^s - \theta_c^m) - \frac{k^s(p_n)}{k^m(p_n) + k^s(p_n)} \mathcal{D}_{mech,c}, \end{aligned} \quad (22)$$

where $k^i(p_n)$ denotes the thermal conduction coefficient dependent on the contact stress [Wriggers and Miehe (1994)], $\mathcal{D}_{mech,c}$ is the contact mechanical dissipation as the plastic slip deformation and it can be written as $\mathcal{D}_{mech,c} = p_\tau \dot{g}_\tau^p$, $p_\tau = \varepsilon_\tau g_\tau^e$. We adopt rate-dependent elastic-plastic model with the elastic domain $E_t := \{p_\tau \in R^{d-1} \mid \phi_c(p_\tau) \leq 0\}$ in the space of the contact tangential stress. The yield functions corresponding to each surface are taken as

$$\phi_c = \|p_\tau\| - p_n \mu_0 \leq 0, \tag{23}$$

where μ_0 is interface frictional coefficient. Fix p_n and use the maximum dissipation principle, $(p_\tau - \tilde{p}_\tau) \cdot \dot{g}_\tau^p \geq 0, \forall \tilde{p}_\tau \in E_t$, so the tangential plastic slip may be given as $\dot{g}_\tau^p = \gamma_c \frac{p_\tau}{\|p_\tau\|}$, γ_c is the plastic parameter. During plastic deformation, the active mechanism must satisfy the consistency condition

$$\gamma_c \geq 0, \quad \gamma_c \phi_c = 0, \tag{24}$$

So the γ_c is uniquely determined by the Eq. 24.

4 Numerical simulations

The FCC polycrystalline body of copper shown in Fig. 2 is simulated, the size is $162nm \times 131nm \times 110nm$. It consists in 4 parts with 16 contact pairs. The body contains 69320 elements and 18689 nodes, the element C3D4T is taken in part 1, 2 and 3 and element C3D8T is adopted in part 4. Elastic constants are taken as: $C_{11} = 168.4GPa$, $C_{12} = 121.4GPa$, $C_{44} = 75.4GPa$, at initial temperature $0^\circ C$, density is $8960kg/m^3$, thermal conductivity is $1.439W/m \cdot ^\circ C$, linear expansion coefficient is $1.7 \times 10^{-5}/^\circ C$, specific thermal capacity is $390J/kg \cdot ^\circ C$, the constants of the pressure dependent contact conductivity relations are given as $0.05W/N \cdot ^\circ C$. The viscous slip parameters are calculated from fitting test curve [Huang (1991)]. It is assumed that within each single crystal there is only one set of slip systems $\{111\} <110>$. In this system, the initial slip hardening modulus $h_0 = 0.5415GPa$, the critical shear stress $\tau_0 = 0.0608GPa$, the stress in the first stage $\tau_s = 0.1095GPa$, coefficient of rate-sensitive hardening factor $\dot{a}^{(\alpha)}$ is taken as 0.001.

4.1 Bending conditions

Boundary conditions at bending state: from Fig. 2, the up surface XOZ and the bottom surface XOZ are subjected to a bending angle 5.7° , on the right surface YOZ the heat flux is $4 \times 10^{14}J/s \cdot m^2$ and temperature on the left surface YOZ is subjected to from $0^\circ C$ to $20^\circ C$, linear increasing with time. Displacements on the near surface XOY equal to zeros, the other surface XOY is free. The initial

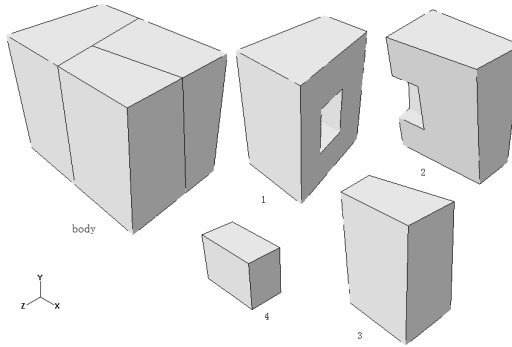


Figure 2: Polycrystalline aggregates and each single crystal.

temperature of finite nodes is 0°C . The fictional coefficients on all contact surfaces are assumed 0.2. Initial meshes and deformed meshes for bending simulation are shown in Fig. 3 (a, b) respectively.

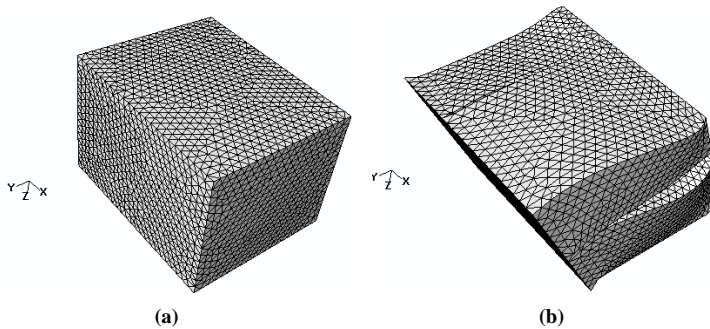


Figure 3: (a) Initial meshes, (b) deformed meshes.

The frictional dissipation ($J \times 10^{-9}$) with time (s) of the polycrystalline body is shown in Fig. 4 (a), external work is shown in Fig. 4 (b), potential energy is shown in Fig. 4 (c) and strain energy in Fig. 4 (d) .

In the case of external forces do work, potential energy and strain energy have changed that causes the plastic dissipation occurred inside the crystal and the separation occurred on the contact interface or a small amount of penetration, the interface sliding making the friction dissipation increase with time.

As all surfaces of the inner part number 4 of the crystals are contact surfaces, here remove crystal 3. Contact pressure contour at different times are shown Fig. 5 (a),

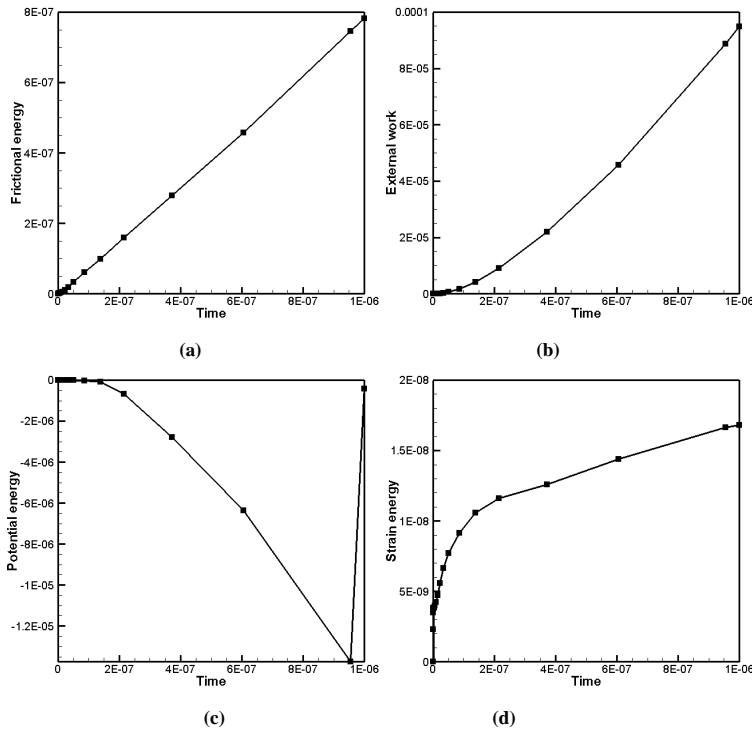


Figure 4: (a) The frictional dissipation, (b) external work, (c) potential energy, (d) strain energy.

(b) and (c), respectively. The displacement jump contour of the contact at different times are shown Fig. 6 (a), (b) and (c).

From contact pressure contour, the contact pressure changes with time, combines with displacement jump contour, it's known that the contact pressure is larger when the displacement jump is smaller. When the contact pressure is limit to zero, the displacement jump reaches to its max value. Here we are concern on the areas of max displacement jump ($m \times 10^{-6}$), next we plot the crack as a function of time in Fig. 7 (a) and difference in temperature ($^{\circ}\text{C}$) of master node and slave node between crystal 3 and crystal 2 in Fig. 7 (b).

There exists a temperature change among bodies through the contact interfaces in addition to the friction heat generation. Due to the change of contact pressure, the heat flux also change with time and results in different temperature on both sides of the contact zone in Fig. 7 (b). If we only conserve crystal 4 and remove other parts of the crystals, the relation of the contact pressure (Gpa) and heat flux ($J \times 10^{-9}$)

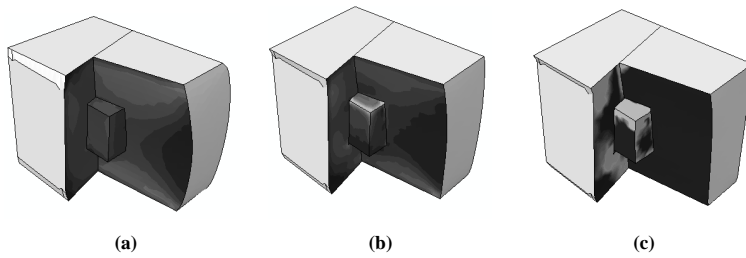


Figure 5: Contact pressure contour at time (a) $4.5 \times 10^{-10}s$, (b) $5 \times 10^{-8}s$, (c) $1 \times 10^{-6}s$.

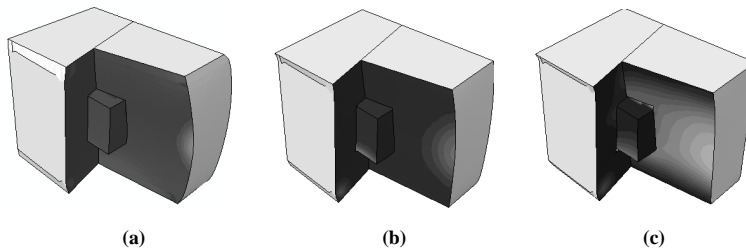


Figure 6: Displacement jump contour at (a) $4.5 \times 10^{-10}s$, (b) $5 \times 10^{-8}s$, (c) $1 \times 10^{-6}s$.

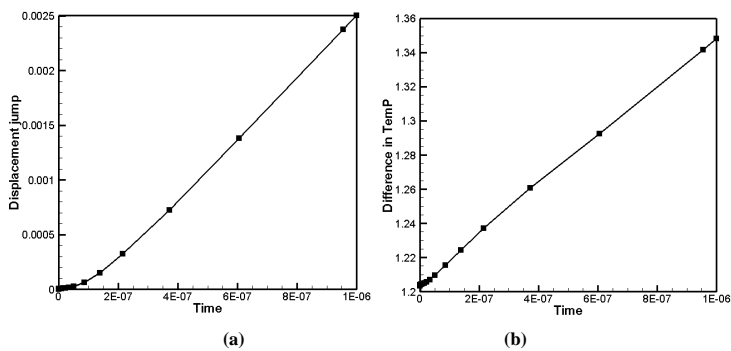


Figure 7: (a) Displacement jump with time, (b) Difference in temperature with time.

can be more clear in the heat flux contour of crystal 4 in Fig. 8.

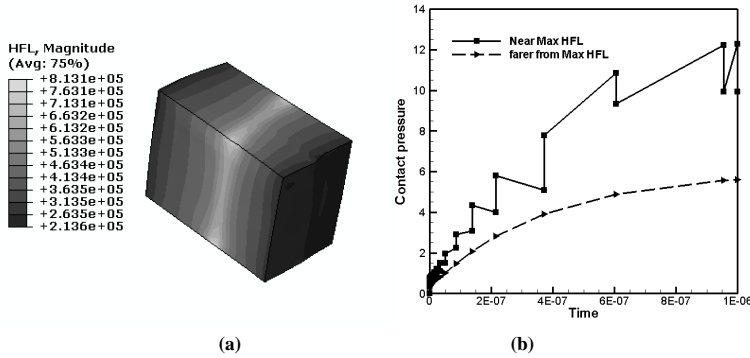


Figure 8: (a) Heat flux contour, (b) Contact pressure with time in the band zones near magnitude HFL and zones more far from the magnitude HFL.

As crystal 4 is surrounded from Fig. 2 view and near middle band zones of that contact with three crystals at the initial time, if the zones separate from one crystal and that may be contact with one of the others. The evolution of contact pressure with respect to time is given in Fig. 8 (b). We see that it is very smooth for low HFL and erratic for high HFL. The effect of continuing slip deformation making the frictional dissipation increasing with the time, at the end time the heat flux in the band zones are larger than other regions, it can be seen from heat flux contour in Fig. 8 (a). Heat flux increases with contact pressure increasing on the contact interfaces compare the results of two different zones near from the magnitude heat flux in Fig. 8 (b).

4.2 Torsion conditions

Boundary conditions at torsion state: the up surface XOZ and the bottom surface XOZ are subjected to torsion angle 2.9° , and other conditions are the same to the bending loading.

The deformed meshes are shown in Fig. 9 (a), and at the max crack between crystal 2 and crystal 3, plot the torsion moment ($N \cdot m \times 10^{-9}$) with time (s) on the contact interface crystal 3 and it is show in Fig. 9 (b) , the relation of the torsion moment and displacement jump ($m \times 10^{-6}$) is shown in Fig. 9 (c) and the displacement jump with time is given in Fig. 9 (d).

At the contact interface between crystal 2 and crystal 3, the displace jumps increase with time in Fig. 9 (d) but torsion moment decreases at first then increases with

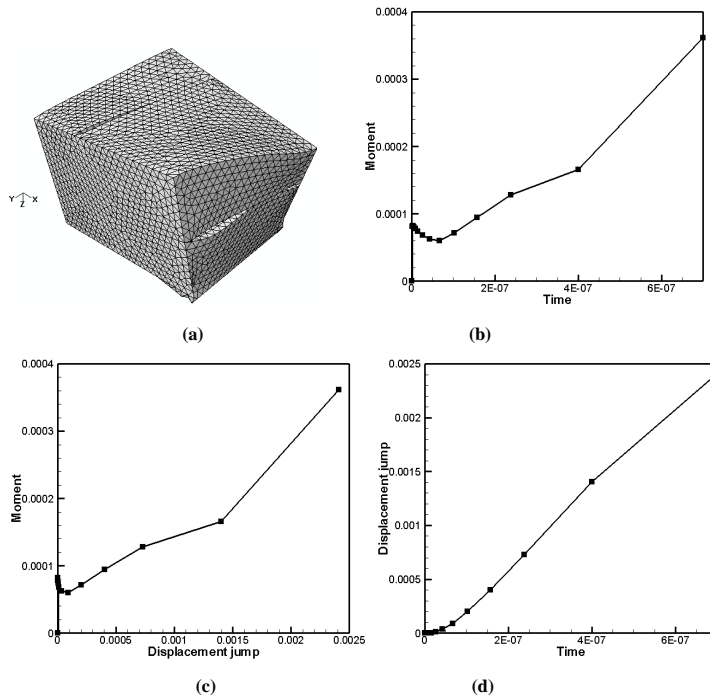


Figure 9: (a) Deformed meshes , (b) torsion moment on the interface of crystal 3,(c) the relation of the torsion moment and displacement jump, (d) the displacement jump with time

time, as torsion moment works there is no crack emerges but has a very small amount of penetration. When there exists penetration, the torsion moment of slave interface decreases. But when the displacement jumps appear and increase, torsion moment always increases with displacement jumps increasing.

The frictional dissipation($J \times 10^{-9}$) with time (s) of the polycrystalline body is shown in Fig. 10 (a), external work is shown in Fig. 10 (b), potential energy is shown in Fig. 10 (c) and strain energy in Fig. 10 (d) .

Similar to bending state, in the case of external work acting, frictional energy increases with time, potential energy and strain energy are change with time.

Remove crystal 3, contact pressure contour at different times are shown Fig. 11 (a), (b) and (c), respectively. The displacement jump contour of the contact at different times are shown Fig. 12 (a), (b) and (c).

The evolution of contact pressure and displacement jump with time are shown re-

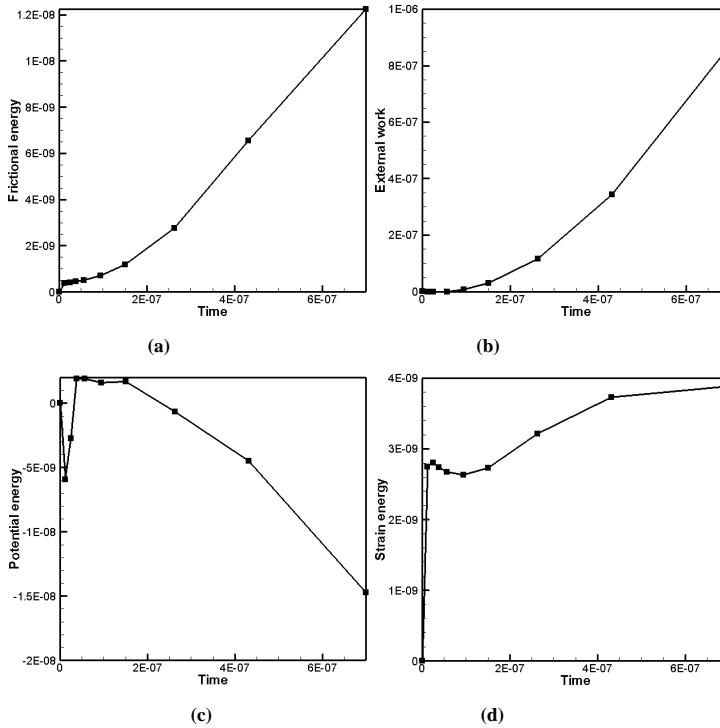


Figure 10: (a) The frictional dissipation, (b) external work, (c) potential energy, (d) strain energy.

spectively in Fig. 11 and Fig. 12 reveals that contact pressure is inverse proportional to displacement jump. Combined with Fig. 5 and Fig. 6, we can conclude that loading in different ways and the path of the crack are not the same.

5 Conclusions

In this paper, a new numerical algorithm for thermal-mechanical coupled behavior of polycrystalline aggregates is presented based on plastic slip theory inside crystals and frictional contact condition on the interfaces between crystals. It involves the mechanics and heat conduction behaviors caused by both force loads and temperature changing in crystal interiors and through contact interfaces. The evolution of the deformation field and the temperature field are typically accompanied with the local rearrangement of material in-homogeneities, it is due to plastic deformation in the crystal interiors and frictional heat generation and heat transfer across the contact interface.

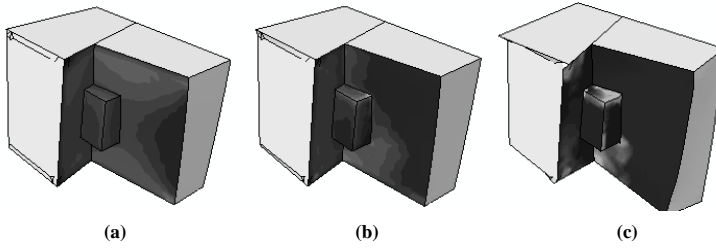


Figure 11: Contact pressure contour at time (a) $2.5 \times 10^{-9}s$, (b) $1 \times 10^{-7}s$, (c) $7 \times 10^{-7}s$.

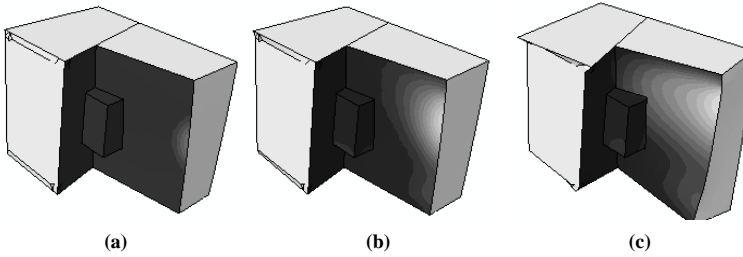


Figure 12: Displacement jump contour at (a) $2.5 \times 10^{-9}s$, (b) $1 \times 10^{-7}s$, (c) $7 \times 10^{-7}s$.

Numerical simulation results for the thermal-mechanical coupled behavior of polycrystalline aggregates shows that crack propagation path is associated with loading ways, temperature change through the contact interfaces besides the friction heat generation. The displacement jumps are related to the interface moment and contact pressure, the torsion moment of slave interface decreases and contact pressure always changes with time. Besides, the friction dissipation energy and strain energy increase with time as the total works of potential energy and external work. The modeling approach in this paper is not limited to several contact bodies, it can be extended to more complicated system with a number of crystals.

Acknowledgement: This work is supported by the Special Funds for National Basic Research Program of China (973 Program 2010CB832702), the National Natural Science Foundation of China (90916027), and also Center for high performance computing of Northwestern Polytechnic University.

References

- Adam, L.; Ponthot, J.** (2002): Numerical simulation of viscoplastic and frictional heating during finite deformation of metal. part i: Theory. *Journal of engineering mechanics*, vol. 128, pp. 1215.
- Adam, L.; Ponthot, J.** (2005): Thermomechanical modeling of metals at finite strains: First and mixed order finite elements. *International journal of solids and structures*, vol. 42, no. 21-22, pp. 5615–5655.
- Anand, L.; Gurtin, M.** (2003): Thermal effects in the superelasticity of crystalline shape-memory materials. *Journal of the Mechanics and Physics of Solids*, vol. 51, no. 6, pp. 1015–1058.
- Belytschko, T.; Liu, W.; Moran, B.** (2000): *Nonlinear finite elements for continua and structures*, volume 36. Wiley.
- Belytschko, T.; Neal, M.** (1991): Contact-impact by the pinball algorithm with penalty and lagrangian methods. *International Journal for Numerical Methods in Engineering*, vol. 31, no. 3, pp. 547–572.
- Chen, Y.; Cui, J.; Nie, Y.; Guan, X.** (2011): The thermo-mechanics coupled model of polycrystalline aggregates based on plastic slip system in crystals and their interfaces. *Advanced Materials Research*, vol. 295-297, pp. 397–405.
- Clayton, J.** (2005): Dynamic plasticity and fracture in high density polycrystals: constitutive modeling and numerical simulation. *Journal of the Mechanics and Physics of Solids*, vol. 53, no. 2, pp. 261–301.
- Huang, Y.** (1991): A user-material subroutine incorporating single crystal plasticity in the abaqus finite element program, mech report 178. *Division of Applied Sciences, Harvard University, Cambridge, MA.*
- Hueber, S.; Wohlmuth, B.** (2009): Thermo-mechanical contact problems on non-matching meshes. *Computer Methods in Applied Mechanics and Engineering*, vol. 198, no. 15-16, pp. 1338–1350.
- Johansson, L.; Klarbring, A.** (1993): Thermoelastic frictional contact problems: modelling, finite element approximation and numerical realization. *Computer methods in applied mechanics and engineering*, vol. 105, no. 2, pp. 181–210.
- Khoei, A.; Biabanaki, S.; Anahid, M.** (2009): A lagrangian-extended finite-element method in modeling large-plasticity deformations and contact problems. *International Journal of Mechanical Sciences*, vol. 51, no. 5, pp. 384–401.
- Khoei, A.; Biabanaki, S.; Vafa, A.; Yadegaran, I.; Keshavarz, S.** (2009): A new computational algorithm for contact friction modeling of large plastic deformation

in powder compaction processes. *International Journal of Solids and Structures*, vol. 46, no. 2, pp. 287–310.

Laursen, T. (1999): On the development of thermodynamically consistent algorithms for thermomechanical frictional contact. *Computer methods in applied mechanics and engineering*, vol. 177, no. 3-4, pp. 273–287.

Laursen, T. (2003): Computational contact and impact mechanics. *Meccanica*, vol. 38, no. 3, pp. 393–394.

Nour-Omid, B.; Wriggers, P. (1986): A two-level iteration method for solution of contact problems. *Computer methods in applied mechanics and engineering*, vol. 54, no. 2, pp. 131–144.

Rosakis, P.; Rosakis, A.; Ravichandran, G.; Hodowany, J. (2000): A thermodynamic internal variable model for the partition of plastic work into heat and stored energy in metals. *Journal of the Mechanics and Physics of Solids*, vol. 48, no. 3, pp. 581–607.

Song, S.; Yovanovich, M. (1987): Explicit relative contact pressure expression-dependence upon surface roughness parameters and vickers microhardness coefficients. In *25th AIAA Aerospace Sciences Meeting*, volume 1.

Temizer, I.; Wriggers, P. (2008): A multiscale contact homogenization technique for the modeling of third bodies in the contact interface. *Computer Methods in Applied Mechanics and Engineering*, vol. 198, no. 3-4, pp. 377–396.

Tian, X.; Cui, J. (2010): Investigations on the deformation behavior of polycrystalline cu nanowires and some factors affecting the modulus and yield strength mode. *Modelling Simul. Mater. Sci. Eng.*, vol. 18, pp. 055011.

Wei, Y.; Anand, L. (2004): Grain-boundary sliding and separation in polycrystalline metals: application to nanocrystalline fcc metals. *Journal of the Mechanics and Physics of Solids*, vol. 52, no. 11, pp. 2587–2616.

Wriggers, P.; Mische, C. (1994): Contact constraints within coupled thermomechanical analysis—a finite element model. *Computer Methods in Applied Mechanics and Engineering*, vol. 113, no. 3-4, pp. 301–319.

Wriggers, P.; Simo, J. (1985): A note on tangent stiffness for fully nonlinear contact problems. *Communications in Applied Numerical Methods*, vol. 1, no. 5, pp. 199–203.